In depth study of the photocatalytic performance of novel catalyst $BaPbFe_2O_6$ for efficient photocatalytic degradation of the dyes

Jeevan Kunwar Chouhan[1], Dushyant Kumar Prajapati[2], Jinesh Menaria[3], Shipra Bhardwaj[4]
[1]*Department of chemistry Government Meera Girls College, MLSU, Udaipur, India,*
[2,3,4]*Department of chemistry Government Meera Girls College, MLSU, Udaipur, India*

***Abstract*—As pollution from industrialization, urbanization, and population growth increases, particularly from the textile industry's dye effluents, pure and drinkable water is becoming rarer and more expensive, prompting interest in innovative solutions like nanomaterials for degrading organic pollutants through photocatalysis. $BaPbFe_2O_6$ photocatalyst showed exceptional performance in degrading Toluidine blue and Basic fuchsin dyes, with superoxide radicals and holes identified as key active species, while maintaining over 86% efficiency after five cycles and minimal metal ion leaching, highlighting their potential for effective wastewater treatment and environmental remediation.**

***Index Terms*—Photocatalyst, dye degradation, wastewater treatment, pollution, toluidine blue dye, basic fuchsin dye**

Graphical Abstract

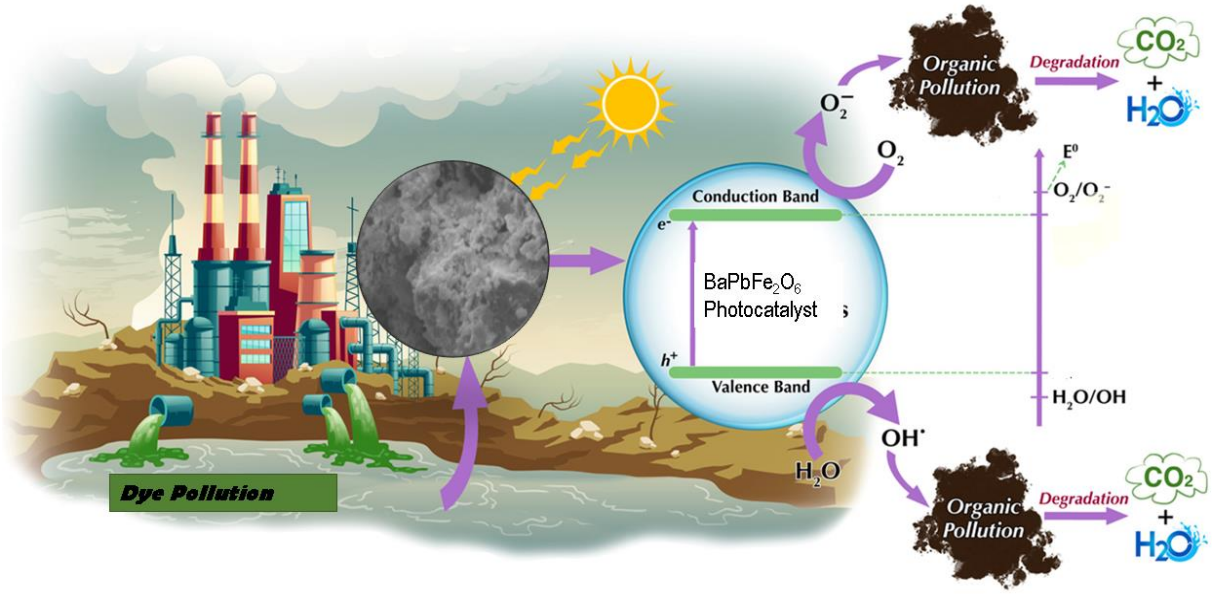

I. INTRODUCTION

The textile industry plays a crucial role in meeting one of humanity's fundamental needs, yet it remains one of the leading contributors to global pollution. These pollutants contain precarious organic and inorganic chemicals which causes water pollution at large scale [(1)].

Due to high demand majority of colored pigments (dyes) are produced by harmful chemicals. A fraction of colored wastewater is discharged into the environment, leading to ecological contamination [(2)].

This discharge is harmful to plants, aquatic life, and humans due to its toxic, cancer-causing, and mutation-inducing properties [3]. Two of such type of dyes triaminotriphenylmethane (Basic Fuchsin) dye and triaminotriphenylmethane (Toluidine Blue) dye are widely used which causes very serious impact on environment if present even in small amounts.

Toluidine Blue (TB) dye is popularly used for staining tissues rich in DNA and RNA, identification of microbiological diseases, such as H. pylori. The substance is highly toxic to humans and can cause long-term health issues in workers who come into contact with the dye, leading to conditions such as anemia, anorexia, weight loss, central nervous system depression and methemoglobinemia [4]. Basic Fuchsin (BF) dye is used to stain muscle, mitochondria, and collagen. Basic Fuchsin's presence in wastewater systems presents significant concerns due to its poor biodegradation, toxicity, carcinogenicity, and unsightliness, necessitating prompt testing and implementation of removal methods [5].

In recent years, there has been significant research dedicated in creating affordable technology for purifying polluted water, with photocatalysis emerging as a successful approach for breaking down harmful pollutants in wastewater [6]. To degrade these toxics from wastewater several methods have been employed. Among them photocatalytic degradation has become increasingly popular because of its affordability and effectiveness [7]. This technology utilizes oxidative processes to generate reactive oxidative species that can interact with organic contaminants in the presence of sunlight [8].

Several technologies including photocatalytic degradation of these dye pollutants. The focus is currently shifting to the discharged water from wastewater treatment plants as a valuable resource for reuse. In this study, the removal of Basic Fuchsin dye and Toluidine Blue dye from aqueous solutions by a newly synthesized $BaPbFe_2O_6$ nanomaterial in sunlight with variable pH, dye concentration, radiation intensity and nanomaterial amount. The semiconducting photocatalyst, which can absorb energy greater than or equal to the energy gap, creates electrons and holes, thereby improving the effectiveness of organic dye oxidizers [9].

Lately, significant advancements in nanotechnology have highlighted the importance of metal oxide nanoparticles (NPs) for a wide range of technological purposes, such as sensors and photocatalysis [10]

BaO nanoparticles (BaO NPs) possess distinctive characteristics, including a highly reactive surface, broad bandgap, narrow emission, and strong electrical conductivity. These properties enable BaO NPs to be utilized in various applications, such as the production of crown glass, humidity sensors, and photocatalysis [11].

Numerous photocatalysts based on BaO have been documented for the degradation of these organic contaminants likewise, $BaAl_2O_4$ [12], $Ba_2NaNb_5O_{15}$ [13] and pervoskite $BaSnO_3$ [14].

Examples of iron oxides commonly found in nature include antiferromagnetic hematite (Fe_2O_3), paramagnetic iron oxide, ferromagnetic iron oxide, ferromagnetic maghemite, and supermagnetic magnetite (Fe_3O_4). The most abundant iron minerals are magnetite, hematite, and maghemite (III)[15]. Iron oxide nanoparticles (Fe_3O_4 NPs) possess several advantageous properties when compared to other types of nanoparticles. These include low toxicity, biocompatibility, cost-effectiveness, and a high surface area to volume ratio [16].

Lead oxide (PbO) possesses several distinctive characteristics that make it suitable for various photocatalytic applications. These characteristics include a low band gap energy, high thermal and stiffness properties, superior tensile strength stability, and appropriate photocatalytic activity. These inclusive features enable lead oxide to effectively meet the requirements of photocatalytic applications [17].

Numerous photocatalysts based on MOF and PbO have been documented for the degradation of organic contaminants such as PbBiO2I-PbO [18], MOF/$CuWO_4$ [19], and Sb_2O_3/PbO [20].

In this study, $BaPbFe_2O_6$ nanomaterial was synthesized using the co-precipitation method and its catalytic effect on the degradation of cationic dyes, toluidine blue, and basic fuchsin under visible light irradiation was investigated. The samples were carefully analyzed using X-ray diffraction (XRD), X-ray photoelectron spectroscopy (XPS), transmission electron microscopy (TEM), photoluminescence (PL) spectroscopy and Brunauer-Emmett-Teller (BET) analysis. The findings showed that the substance could be more extensively examined for the breakdown of additional dyes, the decrease of toxic ions, and the presence of organic substances. The method described

above has led to the development of a highly effective environmentally friendly photochemical material for remediating the environment.

II. MATERIALS AND METHODS

At first, Barium Nitrate, Lead Nitrate, and Iron Nitrate were combined. A suitable quantity of Sodium Hydroxide was then incorporated into the mixture to facilitate precipitation, all while maintaining constant stirring. For the scavenger test, EDTA was employed [21].

III. REAULTS AND DISCUSSION

A. Characterization

The UV-Vis spectra indicate the highest absorbance at 199.2nm with an optical bandgap of approximately 5.45 eV.

The EDX spectrum of $BaPbFe_2O_6$ NPs reveals prominent peaks corresponding to Ba, Pb, Fe, and O elements with weight percentages of 4.83, 5.24, 12.91, and 77.02, respectively, providing strong evidence for the successful synthesis of $BaPbFe_2O_6$ NPs.

The X-ray diffraction (XRD) analysis of $BaPbFe_2O_6$ NPs shows diffraction peaks at 24.03°, 34.38°, 40.93°, 42.21°, and 44.21°, corresponding to the (101), (110), (111), (113), and (103) planes, respectively [22]. The average size of the pure $BaPbFe_2O_6$nanoparticle is found to be 12.31 nm.

The nanomaterials underwent thermal analysis (TGA) at a heating rate of 15 °C/min, and most of the weight loss occurred between 350 °C and 600 °C, indicating the loss of OH.

The reduction in Photoluminescence (PL) intensity is clearly observed, and the PL emission peak is broad, positioned at 471.7, 627.5, and 548.2 nm, due to the direct excitation of $BaPbFe_2O_6$ at the 263.2 nm region [23]. This decrease in intensity is depicted in Figure 4 and is linked to the stabilization of charge carriers [24]. The direct excitation of $BaPbFe_2O_6$ at 263.2nm leads to PL emissions with peaks at 471.7, 627.5, and 548.2 nm.

The XPS spectrum of the synthesized composite nanomaterial exhibits two peaks at 136.7 and 138 eV for Pb $4f_{7/2}$, 711.87 and 724.7 eV for Fe $2p_{3/2}$ and Fe $2p_{1/2}$, and 780.1 and 795.72 eV for Ba $3d_{5/2}$ and $3d_{5/2}$. Additionally, there is a broad peak at 531.23 to 533.27 eV attributed to oxygen vacancies [25].

The BET analysis was utilized for identifying the porosity and morphological characteristics of NPs, as well as for determining the specific surface area of adsorbents [26]. The specific surface area plays a crucial role in determining the performance of catalysts, and usually, a larger specific surface area leads to more significant surface interaction [27].

The BET results for the surface area and possible pore size of the prepared $BaPbFe_2O_6$ are shown in Fig 8. The P/P_o of prepare material is measured as 0.99. The pore volume is calculated as 0.07cc/g with surface area of 18.37 m^2g^{-1}. The pore diameter is calculated as 8.856 nm. It is confirmed from BET results that the prepared $BaPbFe_2O_6$ is capable to adsorb higher quantity of dyes owing to its increases surface area and pore size [28].

B. Photocatalytic degradation of dyes

TB and BF dyes have been used to study the photocatalytic degradation method. Percentage degradation (% D) efficiency of TB and BF has been calculated using $BaPbFe_2O_6$ nanomaterial as comparative study.

The % D (percentage degradation efficiency) has been calculated using standard formula given equation [29]

$$D\% = \frac{A_\circ - A_t}{A_\circ} X\ 100$$

The results obtained for degrading Toluidine Blue (TB) dye for $BaPbFe_2O_6$ was 68.94 % while for Basic Fuchsin nanomaterial exhibited 83.56 % degradation efficiency.

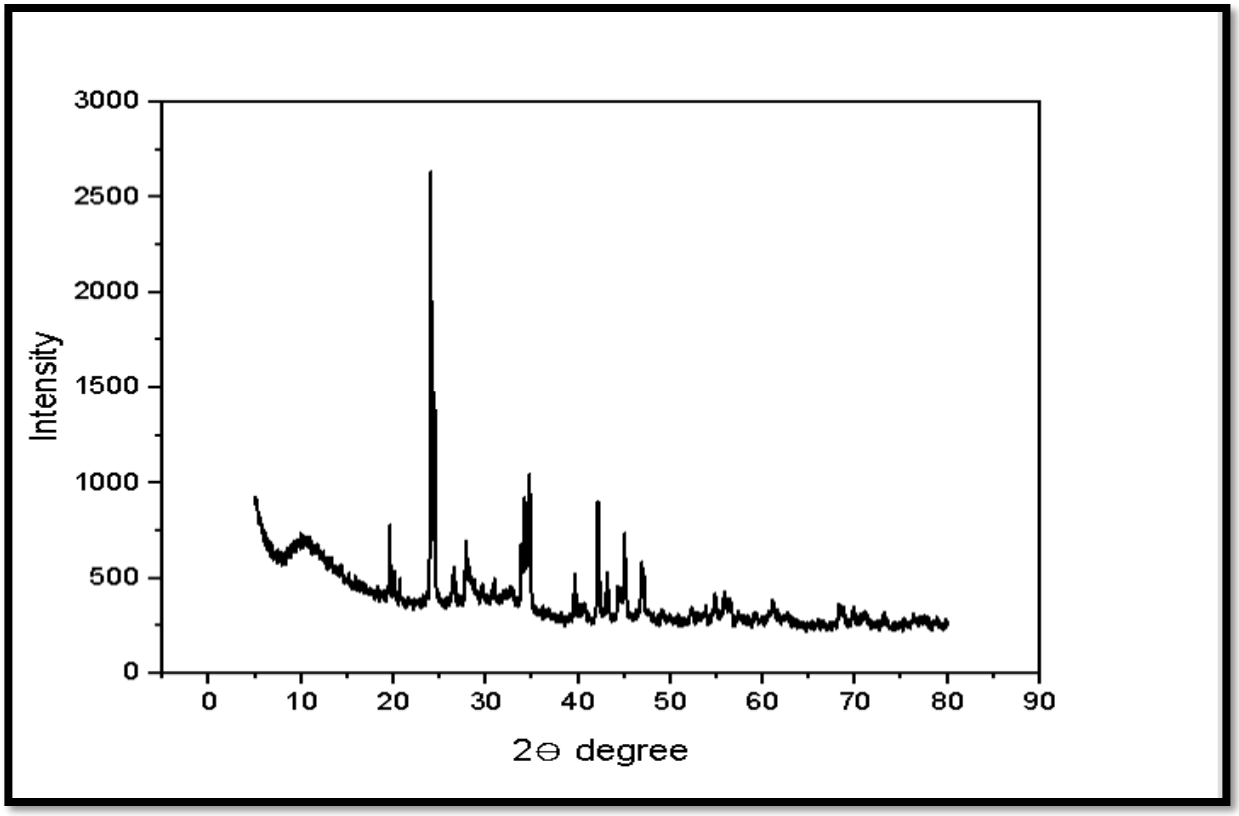

Figure 1: XRD spectra of nanomaterial

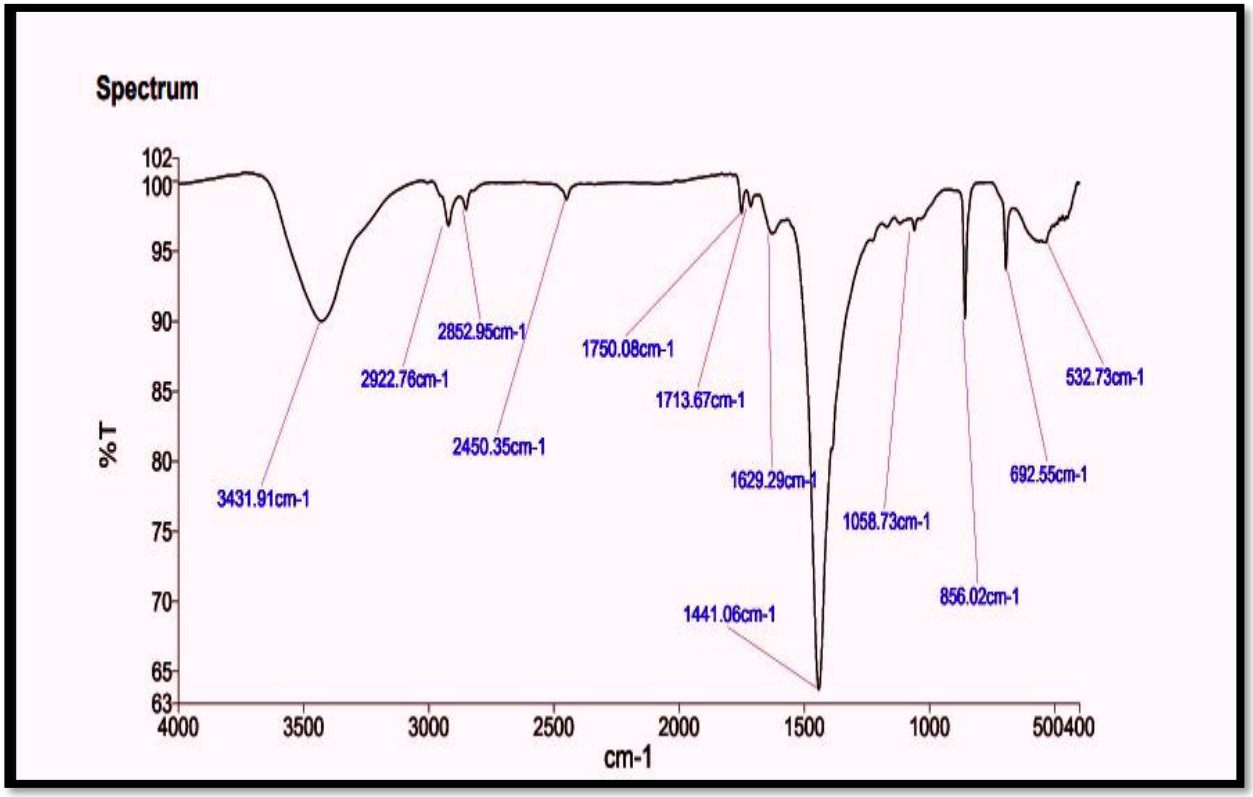

Figure 2: FTIR spectra of nanomaterial

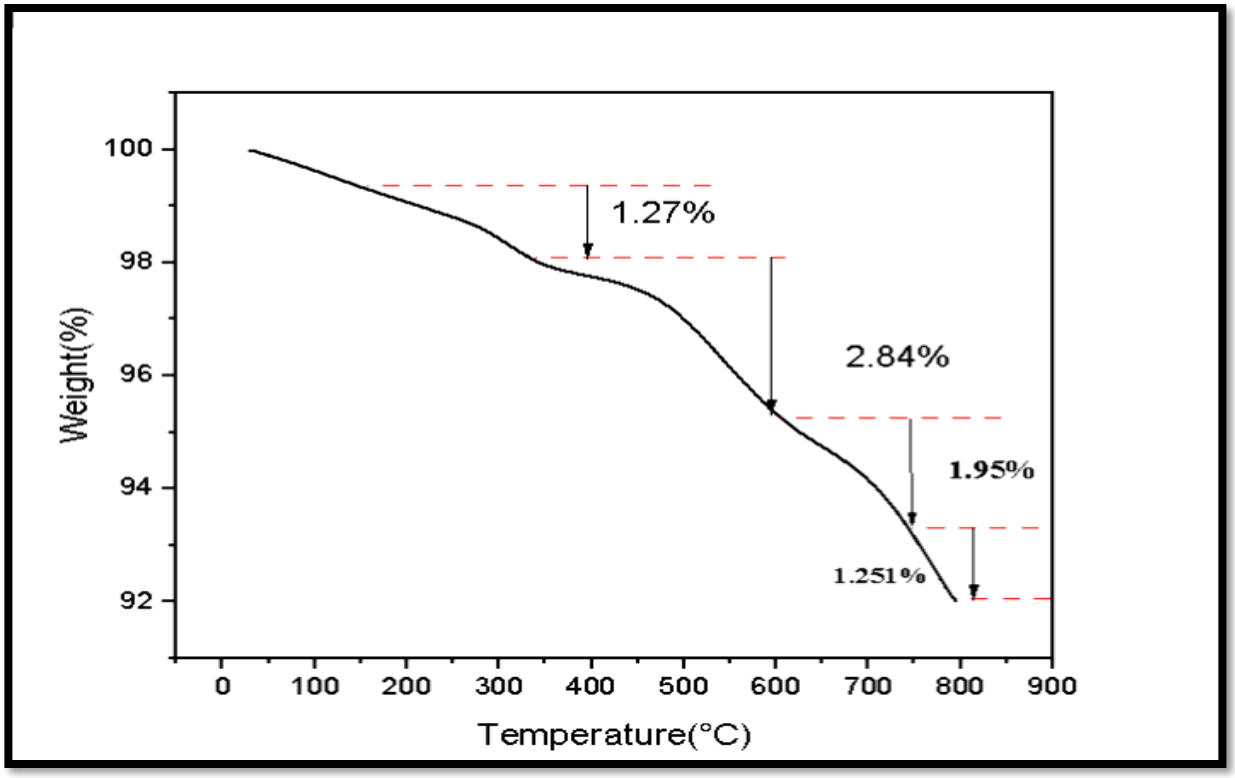

Figure 3: TGA spectra of nanomaterial

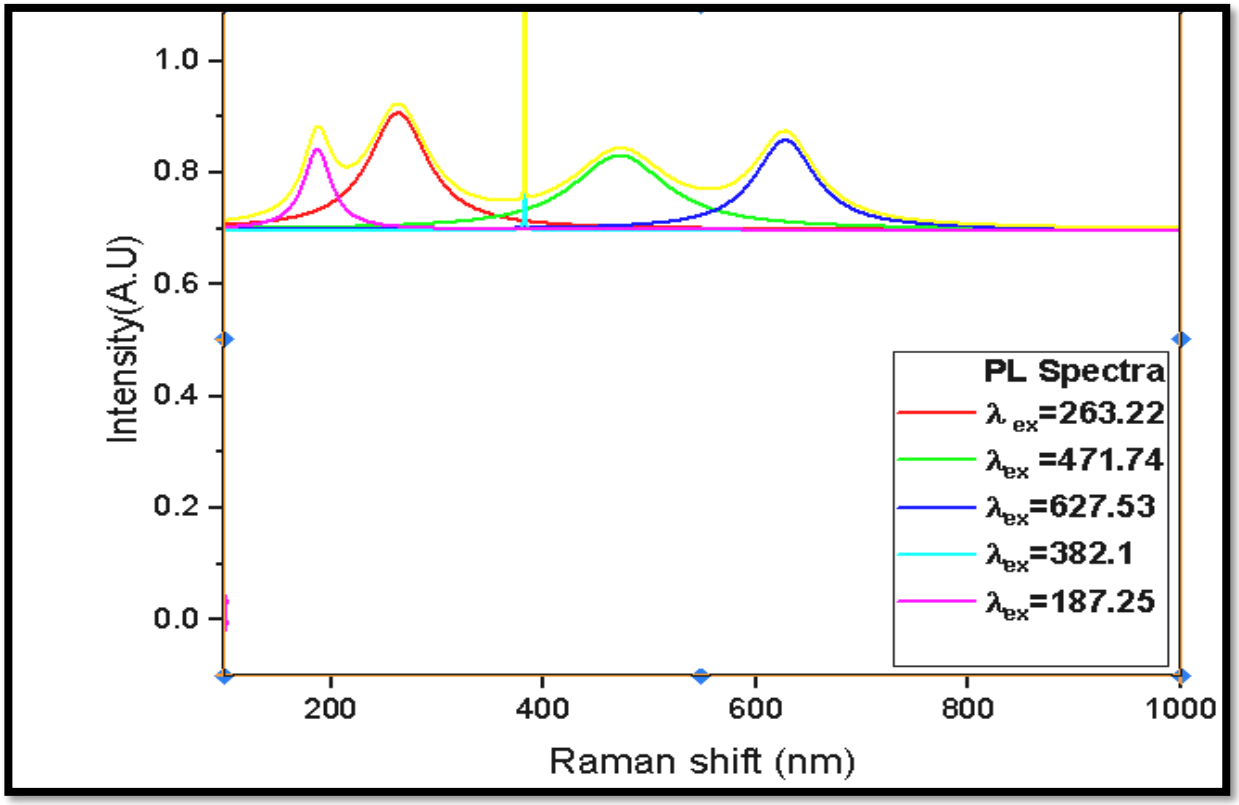

Figure 4: PL intensity of nanomaterial

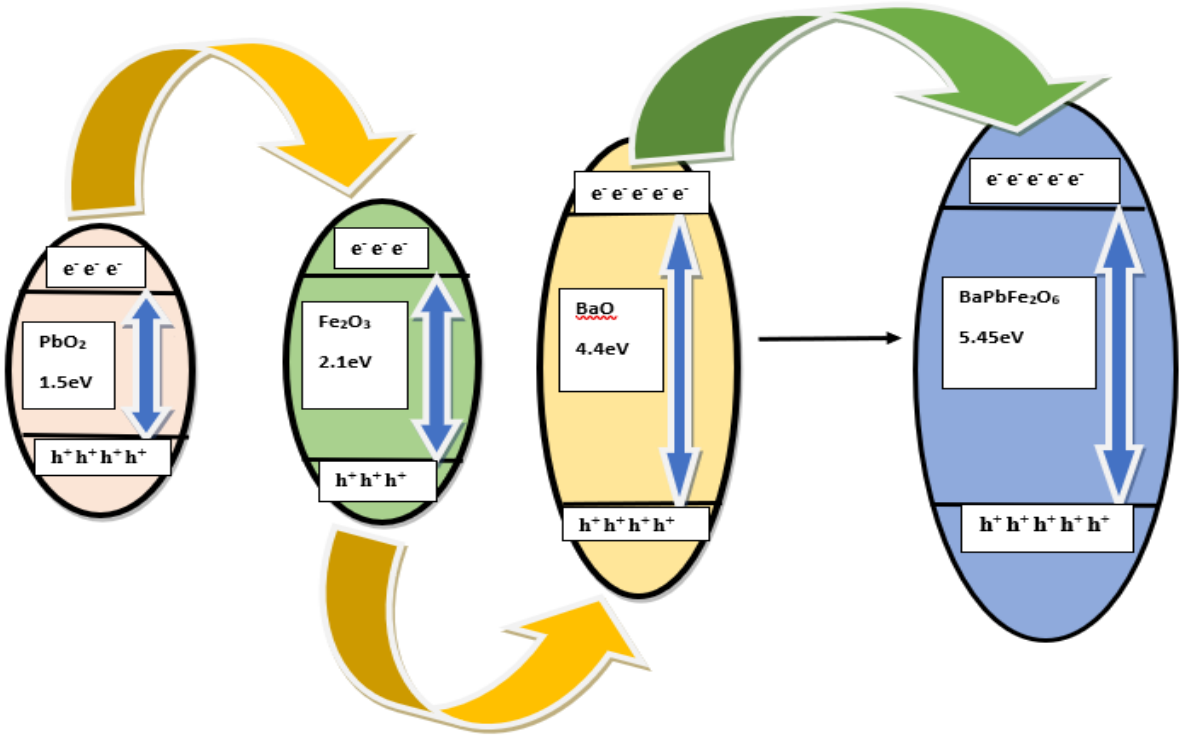

Figure 5: Band gap cascade for prepared photocatalyst

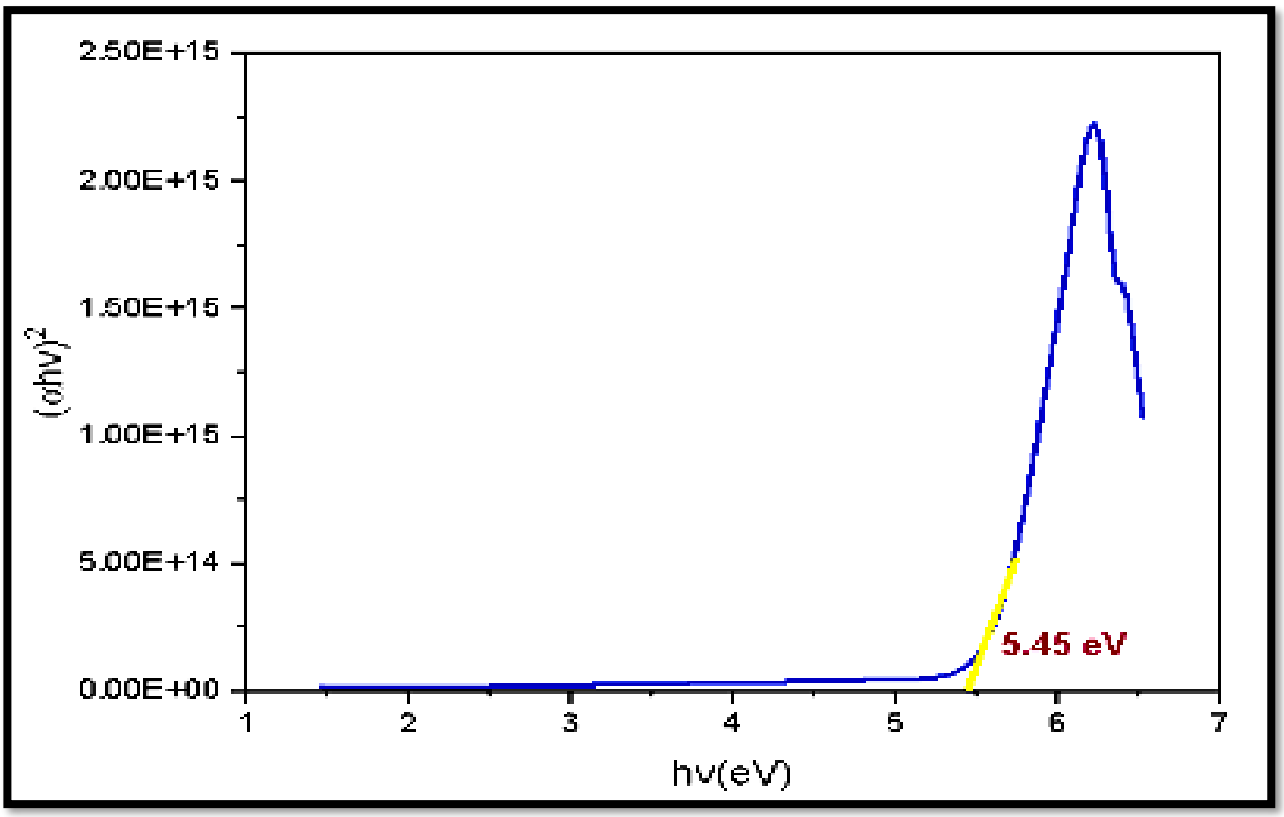

Figure 6: Band gap of nanomaterial

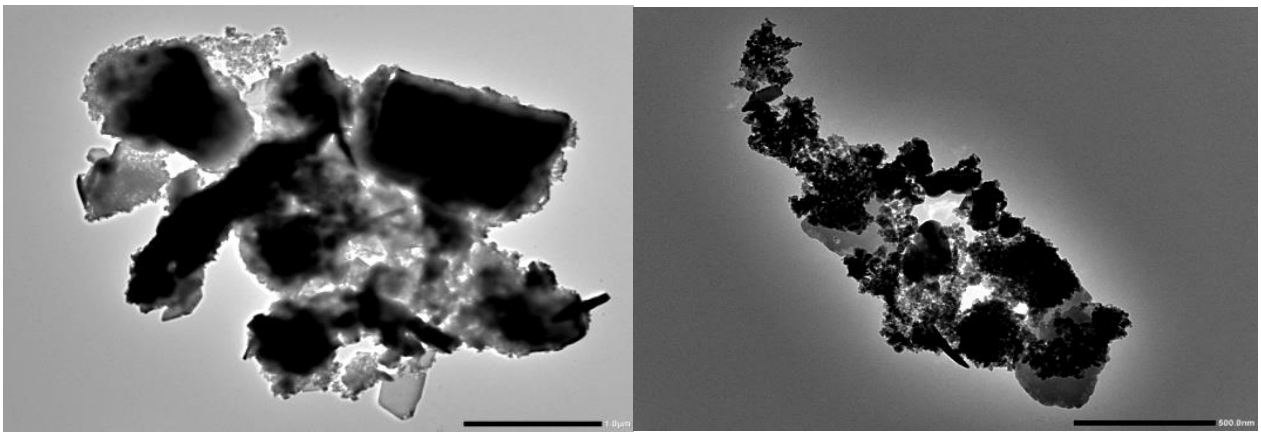

Figure 7: HR-TEM analysis of nanomaterial

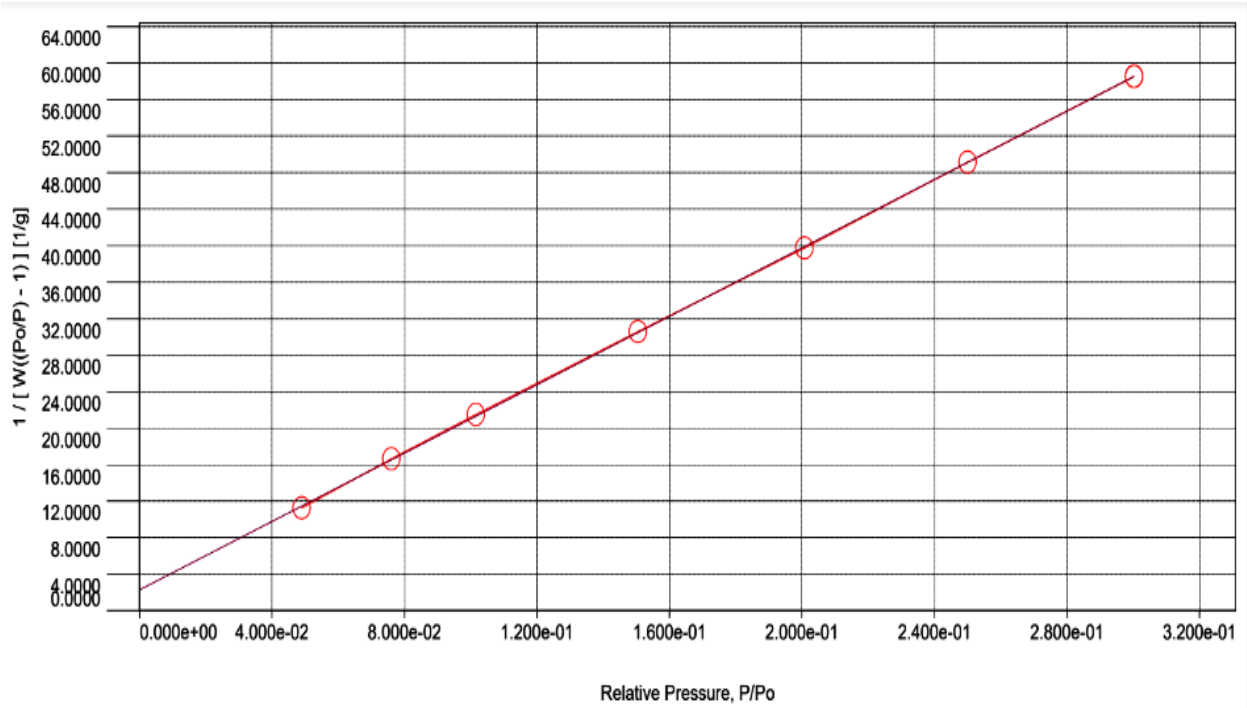

Figure 8: BET analysis of nanomaterial

C. Effect of pH on dye degradation

Figure 9 shows degradation of toluidine blue dye and basic fuchsin with varying pH. It was found that the rate of the degradation reaction for Toluidine Blue increases as the pH level goes up, and that when it hits its peak at pH 10.5, it starts to decline with further increases in pH. In case of Basic Fuchsin dye degradation rate increases till pH 9.5 then it decreases with further increase in pH.

A higher pH value can increase hydroxyl ion concentration, leading to more hydroxyl radicals. A hydroxyl radical can generate a superoxide radical which enhance the photocatalytic decolorization of dyes, with the combined effects of adsorption on the photocatalyst and superoxide radical concentration influencing degradation levels.

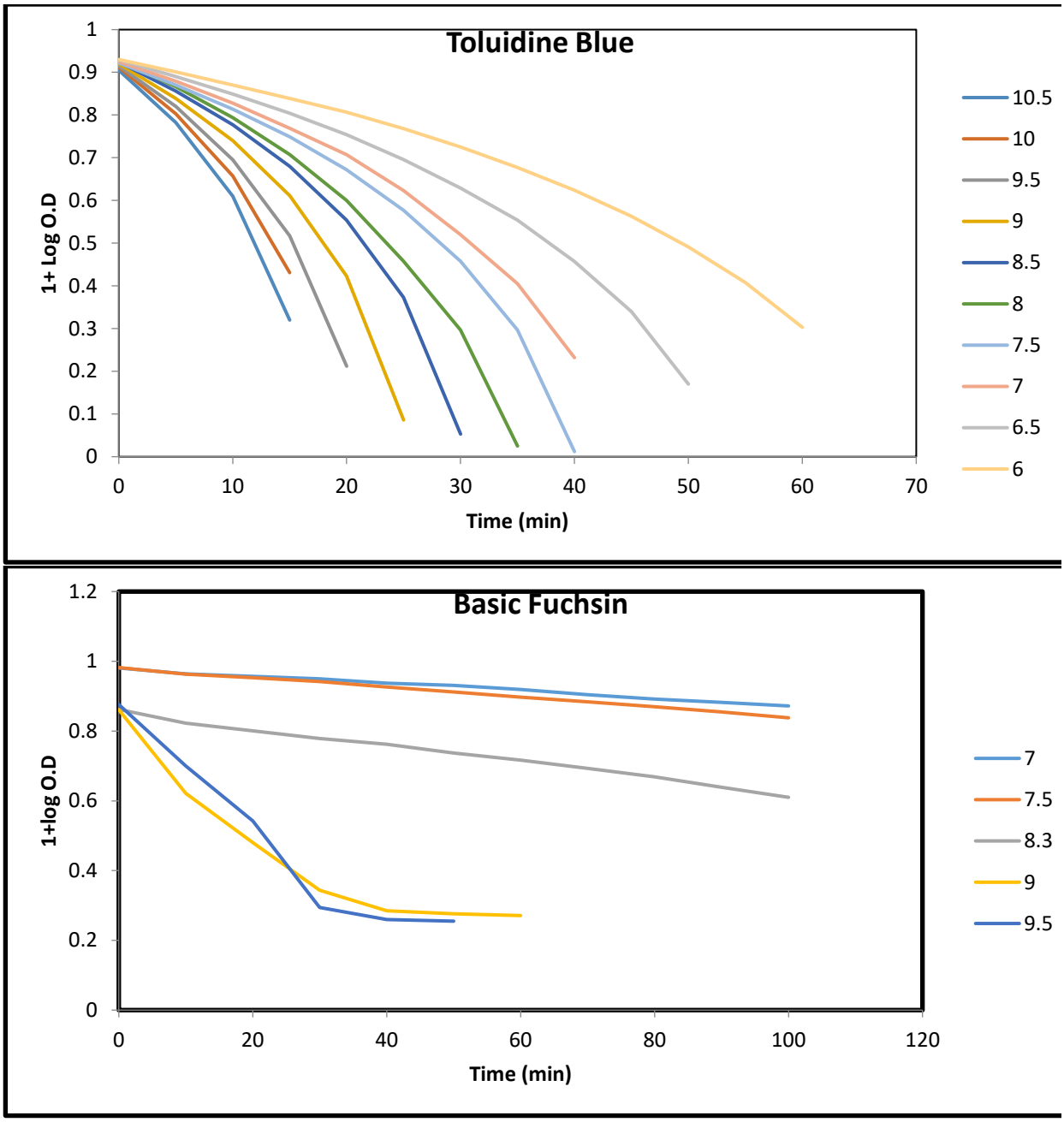

Figure 9: dye degradation with pH variation

D. Effect of dye concentration

The degradation rate was shown to be affected by changes in Toluidine Blue dye concentration 0.4×10^{-5} to 1.8×10^{-5} M while maintaining the same values for all other parameters. Dye concentration for Basic Fuchsin was varied in the range of $0.4\text{x}10^{-4}$ to $1.8\text{x}10^{-4}$. Figure 10 represents the graph of % degradation versus time in different dye concentration with sunlight irradiation. When the amount of dye in the solution goes up, the speed of the reaction goes down because there are more dye molecules around, leading to fewer interactions between the dye molecules and the $O_2^{\cdot-}$ radicals.

As dye concentration rises, the interference from intermediates created during the degradation of the original dye molecules become more significant, amplifying the suppression effects associated with higher concentrations of degradation intermediates.

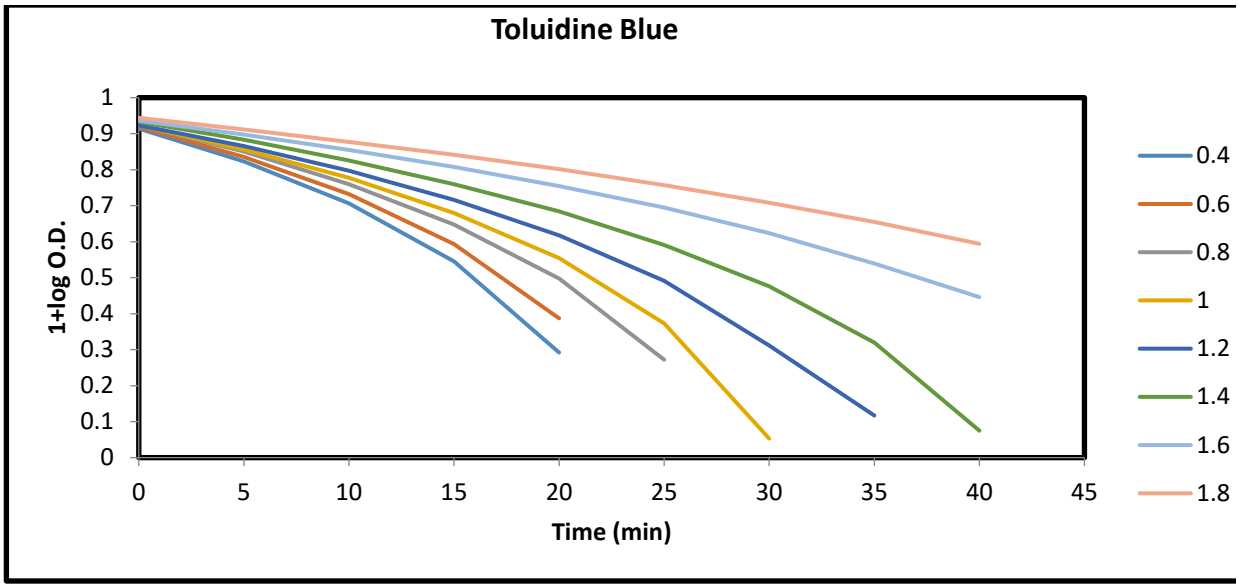

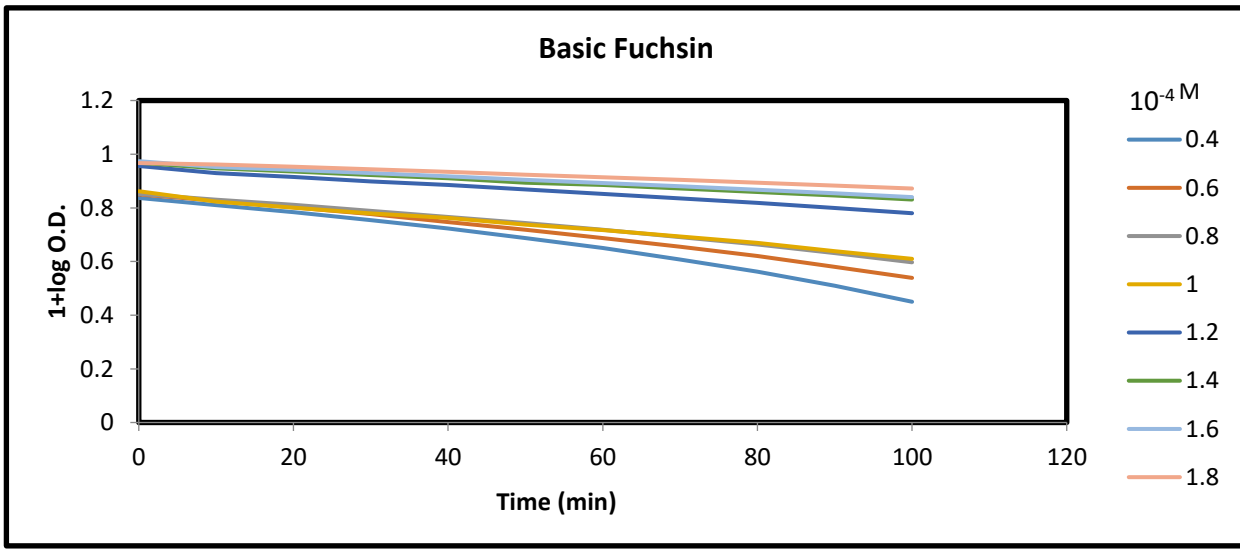

Figure 10: dye degradation with dye concentration variation

E. Effect of amount of catalyst

Determining the optimal catalyst loading is crucial in photocatalytic studies to prevent excessive use of the catalyst. Other parameters remaining the same, various amount of catalyst changes the rate of dye discoloration in the range of 0.04g to 0.16 g.

The effect of different amounts of catalyst loading on the photocatalytic degradation percentage was tested and shown in Figure 11. When $BaPbFe_2O_6$ is exposed to light energy equal to or exceeding its bandgap, electrons are excited from the valence band to the conduction band, creating holes in the valence band; these excited states can either recombine or interact with adsorbed species on the semiconductor surface, leading to the formation of reactive hydroxyl radicals and superoxide radical anions.

$BaPbFe_2O_6 + hv\ (UV) \rightarrow e_{cb}^{-} + h_{vb}^{+}$

$h_{vb}^{+} + H_2O \rightarrow H^{+} + {}^{\cdot}OH$

$e_{cb}^{-} + O_2 \rightarrow O_2^{\cdot}$

$O_2^{\cdot -} + {}^{\cdot}OH + dye \rightarrow degraded\ product$

The percentage of degradation of TB was decreased from 96.4%, 96.15%, and 94.6% with the increased amount of loading of 0.16, 0.14, and 0.12 g, respectively. The percentage of degradation of BF was decreased from 83.79%, 70.62%, and 63.54% with the increased amount of loading of 0.16, 0.14, and 0.12 g, respectively.

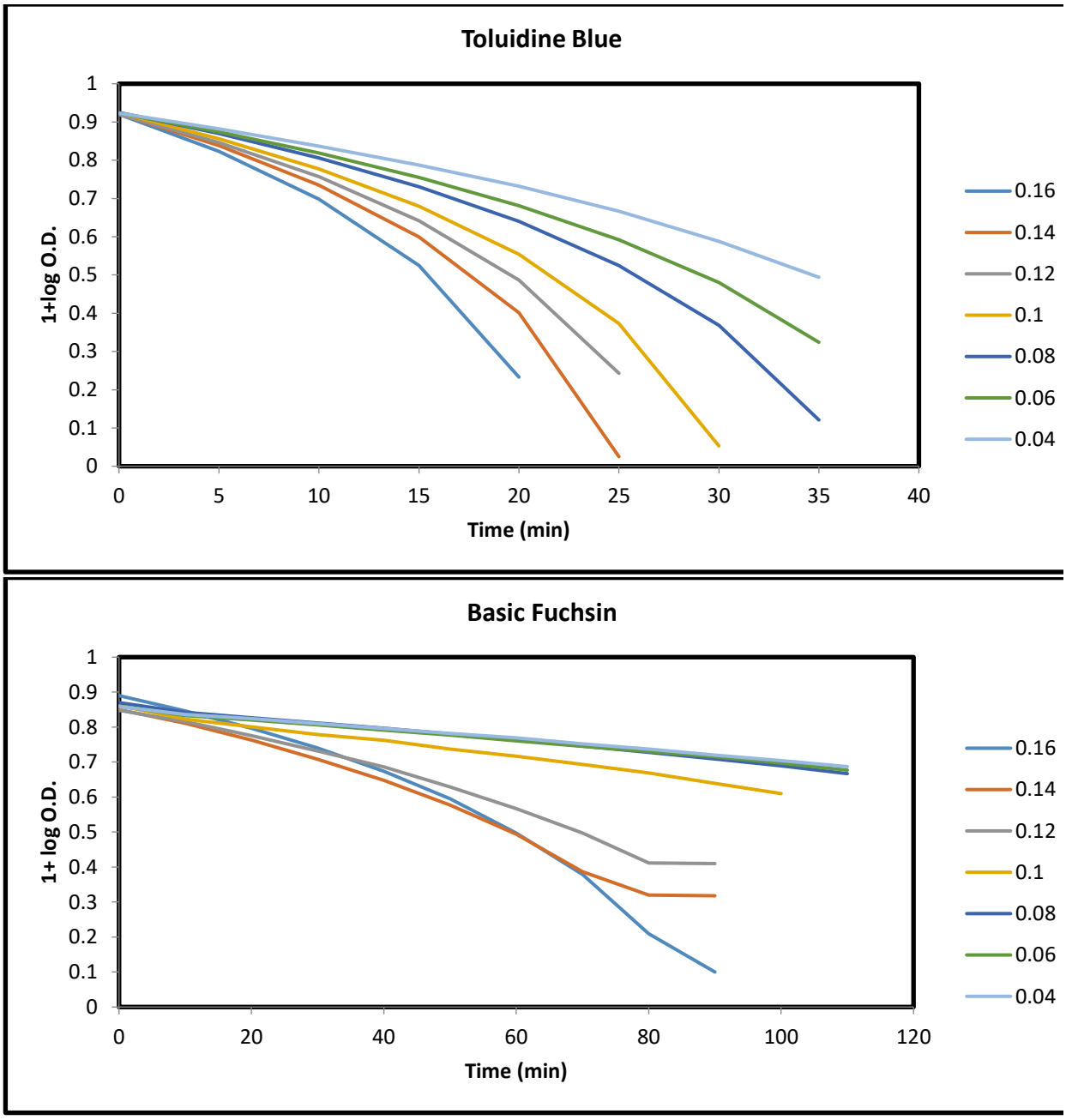

Figure 11: dye degradation with semiconductor variation

F. Effect of light intensity

Assuming all other factors remain the same, the impact of varying light intensity on the speed of color deterioration was also investigated for $BaPbFe_2O_6$. The graph illustrates the percentage degradation as a function of sunlight exposure duration under various light intensities. According to the data, there is a direct correlation between the irradiation intensity and the reaction rate of degradation. The catalyst demonstrated its highest rate of degradation at 1850 $mWcm^{-2}$. This can be attributed to the increase in irradiation intensity leading to a higher number of photons/quanta reaching the catalyst's surface area. This results in a more efficient degradation process of dye molecules. Furthermore, the avoidance of increased light intensity is recommended due to the potential for thermal side reactions caused by additional light exposure.

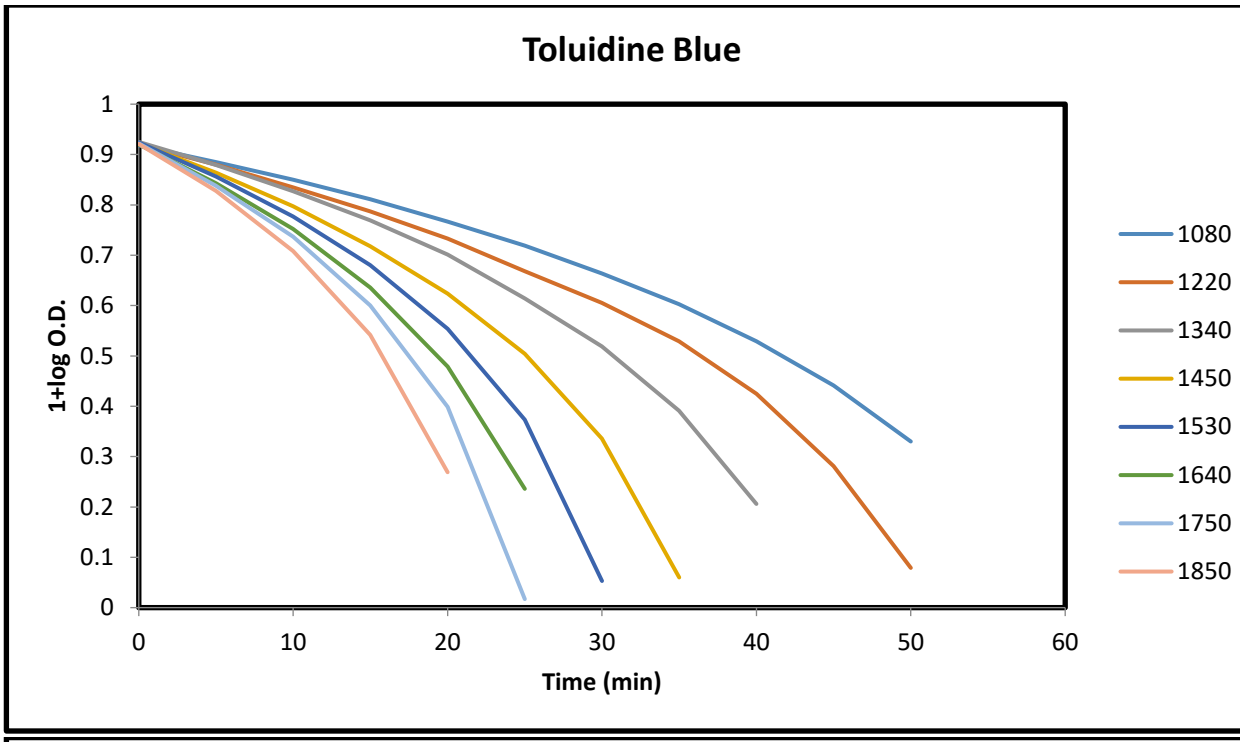

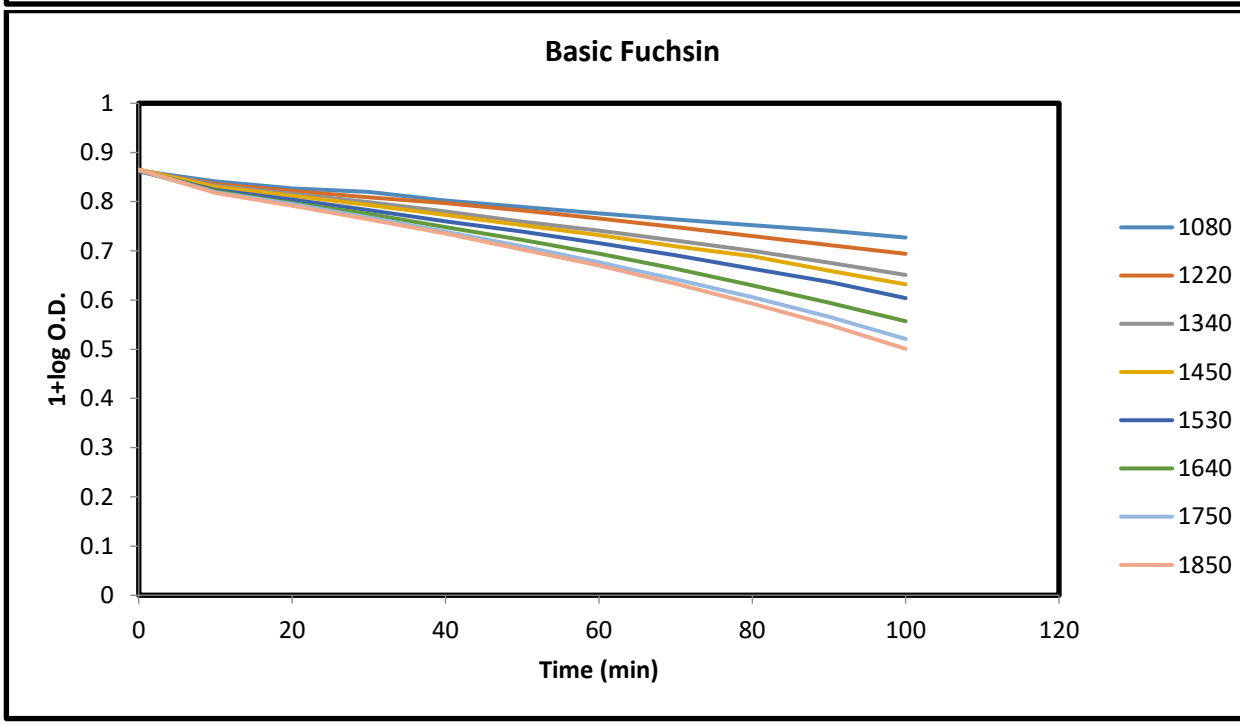

Figure 12: dye degradation with intensity variation

G. Effect of Scavenger on the Photocatalytic Degradation Efficiency of the Dye:

The efficiency of breaking down photocatalytic dyes through products relies on how well electron-hole pairs (e^-/h^+) can be separated to produce active species such as superoxide and hydroxyl radicals ($\bullet O^{2-}$ and $^{\bullet}OH^-$). EDTA has been utilized to scavenge superoxide ($\bullet O^{2-}$) radicals. When employing 5 ml of 1N EDTA with the nanomaterial $BaPbFe_2O_6$, the degradation of toluidine blue dye resulted in only 2.70 % of the dye. In the presence of EDTA scavenger only, basic fuchsin dye degrades by just 1.97%.

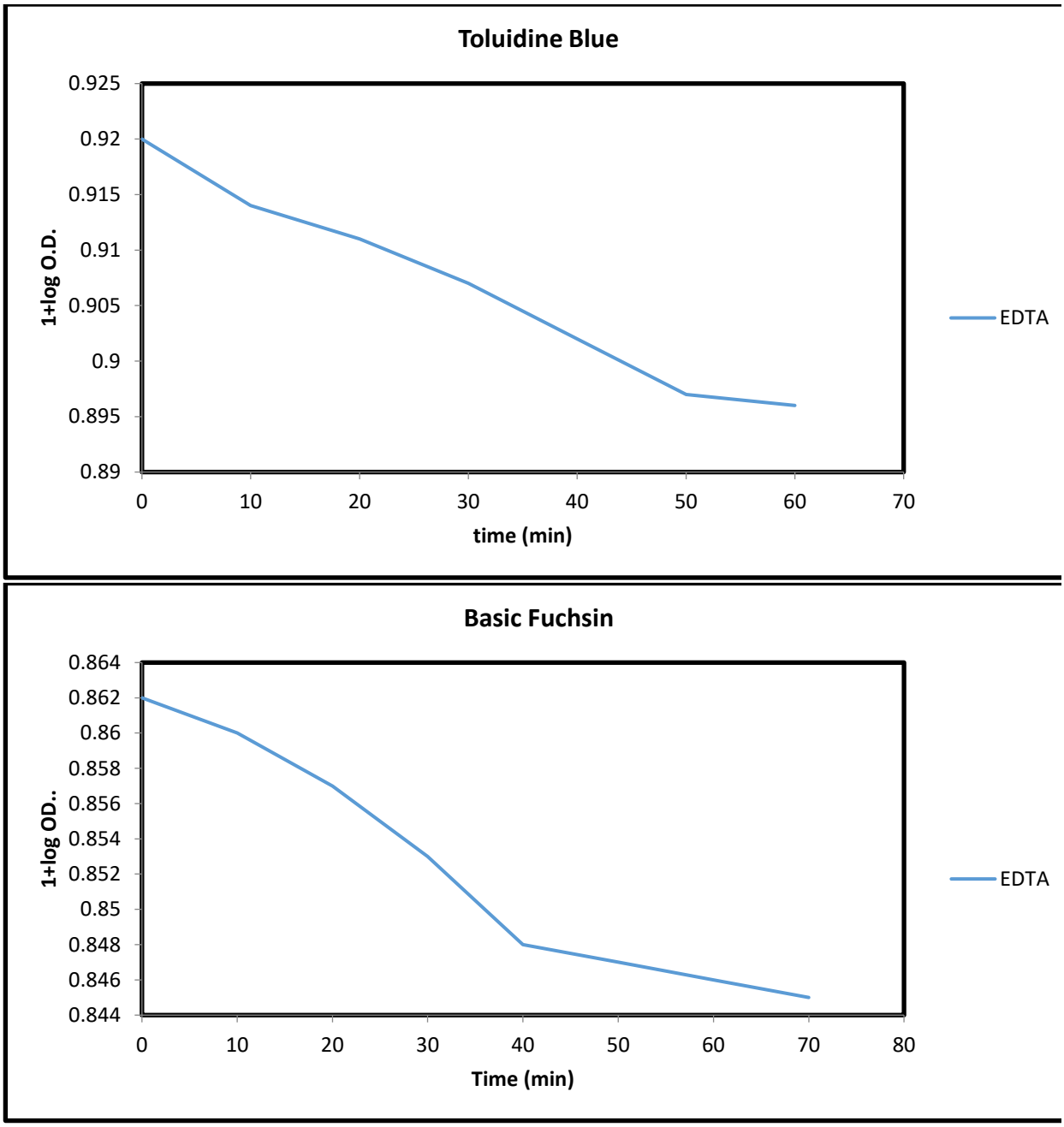

Figure 13: scavenger test for dyes

H. Mechanism of toluidine blue dye degradation

The simultaneous monitoring of the dye solution's chromatographic separation on 2 min intervals of photocatalytic treatment revealed significant decolorization and degradation of the dye, as evidenced by the reduction of its visible and UV bands and the emergence of new compounds, which were characterized through mass spectrometric analysis.

To study the degradation of TB dye under visible light, liquid chromatography-mass spectrometry (LC-MS) was employed to identify its photodegradation byproducts as illustrated in Fig.13, leading to a proposed degradation pathway in Fig. 14, where TB dye remained the primary component, during the dark adsorption phase with no detectable peaks at higher m/z ratios, suggesting no further degradation or polymerization occurred.

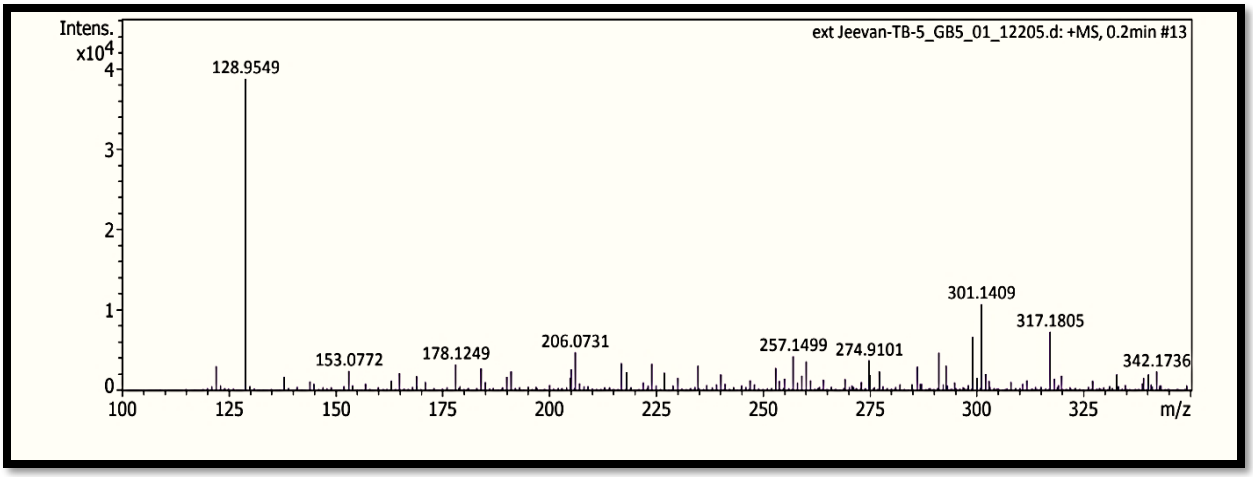

Figure 14: LC-MS spectra of the observed products under visible light

Figure 15: Proposed degradation pathway of TBO dye under visible light irradiation followed by the identification of several intermediates by LC-MS spectral techniques

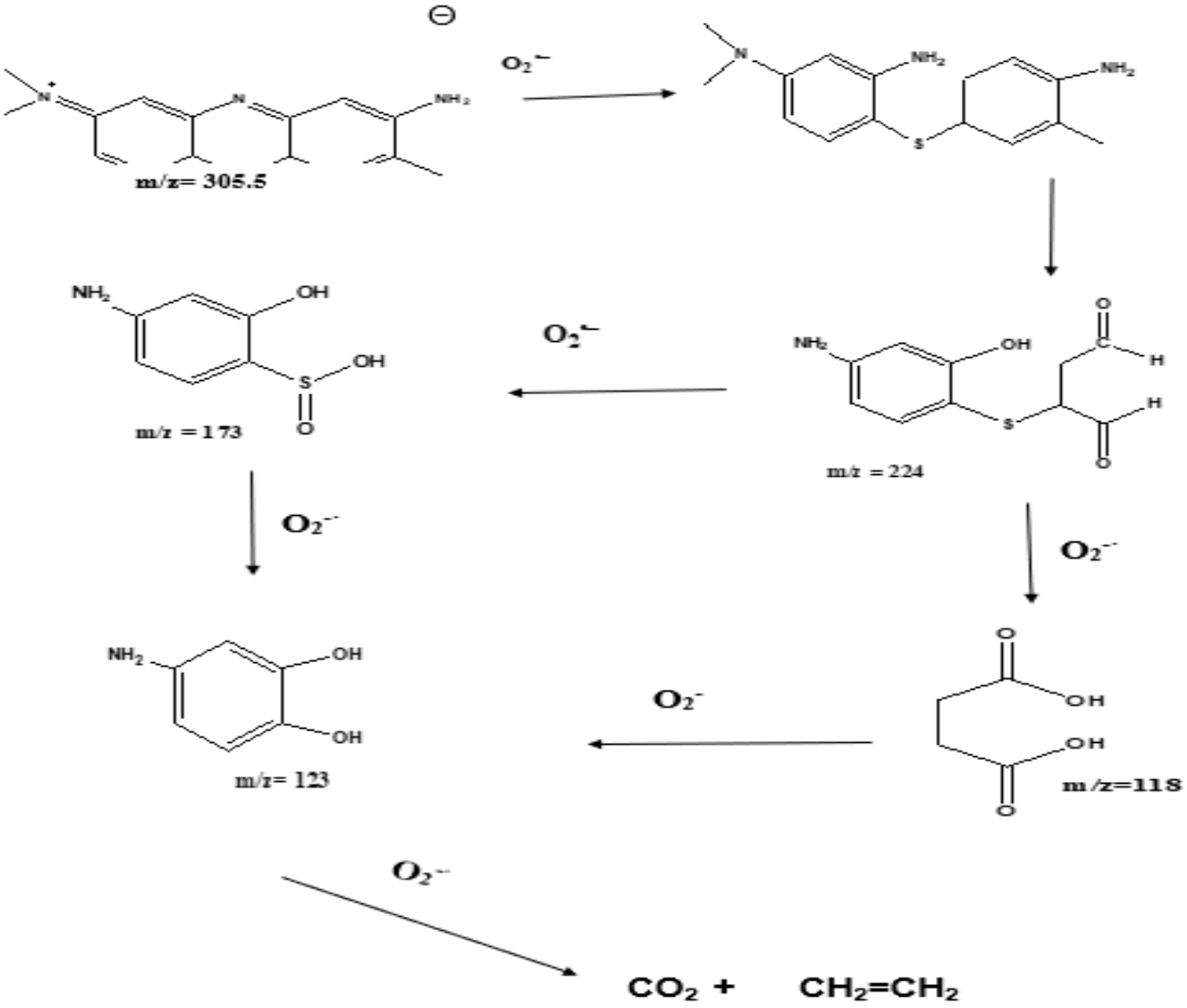

IV. CONCLUSION

The co-precipitation method was used to produce $BaPbFe_2O_6$ nanoparticles, and their structure and morphology were analyzed using various techniques including XRD, FE-SEM, EDS, XPS, HR-TEM, and UV-VIS-NIR, revealing an average grain size of 12.31 nm and the formation of regular small spherical/cylindrical particles. At high light intensity, the photo degradation rate increases as the pH rises to an optimal level when the initial dye concentration is low. In the heterogeneous photocatalytic process, $O_2^{\cdot-}$ radicals react with dye molecules, breaking them down into smaller particles like H_2O, CO_2, and NO_3^- ions.

A. List of Abbreviations
TB: Toluidine Blue
BF: Basic Fuchsin
XRD: X-ray diffraction
FE-SEM: Field Emission Scanning Electron Microscopy
EDS: Energy Dispersive Spectroscopy
XPS: X-ray photoelectron spectroscopy
HR-TEM: High Resolution Transmission Electron Microscopy
UV-VIS/NIR: ultraviolet-visible-near infrared
TGA: Thermogravimetric analysis
BET: Brunauer–Emmett–Teller
PL: Photoluminescence

B. Availabilty Of Data and Materials:
All data is original.

C. Declarations of Interest
None

REFERENCES

[1] Uma, P. I., Shenoy, U. S., & Bhat, D. K. (2023). Electronic structure engineering of BaTiO3 cuboctahedrons by doping copper to enhance the photocatalytic activity for environmental remediation. Journal of Alloys and Compounds, 948, 169600

[2] Kishor, R., Purchase, D., Saratale, G. D., Saratale, R. G., Ferreira, L. F. R., Bilal, M., and Bharagava, R. N. (2021). Ecotoxicological and health concerns of persistent coloring pollutants of textile industry wastewater and treatment approaches for environmental safety. Journal of Environmental Chemical Engineering, 9(2), 105012.

[3] Geng-Sheng Lin, Wenbo Peng, Ji Gao, Abigael Wahlen, Zhaohui Tong, (2023) Functional naturally derived materials to improve the environment: Chemical structures, modifications, applications, and future perspectives: Adv in Bioenergy 8, 93-144

[4] Venkatesan, D., Umasankar, S., Mangesh, V. L., Krishnan, P. S., Tamizhdurai, P., Kumaran, R., & Baskaralingam, P. (2023). Removal of Toluidine blue in water using green synthesized nanomaterials. South African Journal of Chemical Engineering, 45(1), 42-50.

[5] El Haddad, M. (2016). Removal of Basic Fuchsin dye from water using mussel shell biomass waste as an adsorbent: Equilibrium, kinetics, and thermodynamics. Journal of Taibah University for Science, 10(5), 664-674.

[6] Ambaye, T. G., Djellabi, R., Vaccari, M., Prasad, S., Aminabhavi, T., & Rtimi, S. (2023). Emerging technologies and sustainable strategies for municipal solid waste valorization: Challenges of circular economy implementation. Journal of Cleaner Production, 138708.

[7] Xie, C. Z., Luo, R., Gao, Q., Zhang, X., Zhang, D. M., Fan, Y. H., and Shao, F. (2024). Photocatalytic degradation of dyes and magnetic properties in two one-dimensional coordination polymers. Polyhedron, 250, 116825.

[8] Brillas, E., & Oliver, R. (2024). Development of persulfate-based advanced oxidation processes to remove synthetic azo dyes from aqueous matrices. Chemosphere, 141766.

[9] Basavanagoudra, H., Jangannanavar, V. D., Patil, M. K., Inamdar, S. R., & Goudar, K. M. (2024). Barium oxide nanorods: Catalyst concentration and surface defects' role in degrading methylene blue organic pollutant. Chemical Physics Impact, 8, 100578.

[10] Linic, S., Aslam, U., Boerigter, C., & Morabito, M. (2015). Photochemical transformations on plasmonic metal nanoparticles. Nature materials, 14(6), 567-576.

[11] Renukadevi, R., Sundaram, R., & Kasinathan, K. (2020). Barium oxide nanoparticles with robust catalytic, photocatalytic and humidity sensing

properties. Journal of Nanostructures, 10(1), 167-176.

[12] Faisal, S., Majid, S. S., Ahad, A., Sofi, F. A., Mohanta, S., Gupta, M., ... & Shukla, D. K. (2024). Photocatalytic Activity of BaAl2O4 for Water Purification. Langmuir, 40(16), 8418-8426.

[13] Tiwari, S., Gaur, A., Al Huwayz, M., Alrowaili, Z. A., Al-Buriahi, M. S., Vaish, R., & Chauhan, V. S. (2024). Multicatalytic dye degradation capability of Ba2NaNb5O15 ferroelectric ceramics. Proceedings of the Indian National Science Academy, 90(1), 102-112.

[14] Bimli, S., Mulani, S. R., Choudhary, E., Manjunath, V., Shinde, P., Jadkar, S. R., & Devan, R. S. (2024). Perovskite BaSnO3 nanoparticles for solar-driven bi-functional photocatalytic activity: PEC water splitting and Wastewater treatment. International Journal of Hydrogen Energy, 51, 1497-1507.

[15] Jassal V, Shanker U, Gahlot S (2016) Green synthesis of some iron oxide nanoparticles and their interaction with 2-amino, 3-amino and 4-aminopyridines. Mater Today Proc 3(6):1874–1882)

[16] Abdullah JAA, Salah Eddine L, Abderrhmane B, AlonsoGonzález M, Guerrero A, Romero A (2020) Green synthesis and characterization of iron oxide nanoparticles by pheonix dactylifera leaf extract and evaluation of their antioxidant activity. Sustain Chem Pharm 17:100280. https://doi.org/10.1016/j.scp.2020. 100280

[17] Khorrami, M. A., Sohrabnezhad, S., & Asadollahi, A. (2024). Enhanced visible-light-active MOF-based PbO photocatalyst for binary dye decolorization: A comprehensive study. Journal of Molecular Liquids, 402, 124722.

[18] Liu, F. Y., Lin, J. H., Dai, Y. M., Chen, L. W., Huang, S. T., Yeh, T. W., and Chen, C. C. (2018). Preparation of perovskites PbBiO2I/PbO exhibiting visible-light photocatalytic activity. Catalysis Today, 314, 28-41.

[19] Ramezanalizadeh, H., & Manteghi, F. (2018). Synthesis of a novel MOF/CuWO4 heterostructure for efficient photocatalytic degradation and removal of water pollutants. Journal of Cleaner Production, 172, 2655-2666.

[20] Wang, Z., Srivastava, V., Iftekhar, S., Ambat, I., & Sillanpää, M. (2018). Fabrication of Sb2O3/PbO photocatalyst for the UV/PMS assisted degradation of carbamazepine from synthetic wastewater. Chemical Engineering Journal, 354, 663-671.

[21] Chouhan J.K.,Prajapati D.K., Bhardwaj S.,(2023) Synthesis of BaPbFe2O6 nanoparticles and its novel application as a catalyst for the photodegradation of crystal violet dye", Int Journal of Research and Analytical Reviews (IJRAR), E-ISSN 2348-1269, P- ISSN 2349-5138, Vol.10, Issue 1, pp.699-708.

[22] Naz, F., Saeed, K. Synthesis of barium oxide nanoparticles and its novel application as a catalyst for the photo degradation of malachite green dye. Appl Water Sci 12, 2022, 121.

[23] Zhao, H., Xin, X., Wang, Q., Wang, Z., Wang, Y., Cheng, Q., ... & Jiang, P. (2024). Mn5+-doped BaAl2O4, Ba3Al2O6, and Ba7Al2O10 phosphors emitting in the second near-infrared biological window. Journal of Alloys and Compounds, 976, 173044.

[24] Borja-Urby, R., Díaz-Torres, L. A., Salas, P., Moctezuma, E., Vega, M., & Ángeles-Chávez, C. Structural study, photoluminescence, and photocatalytic activity of semiconducting BaZrO3: Bi nanocrystals. Materials Science and Engineering: B, 176(17), 2011, 1382-1387.

[25] Saber, I., Dahmani, K., Galai, M., Magri, A. E., Hsissou, R., Barbita, H., and Elyoubi, M. S. (2024). Synthesis and characterization of new eco-friendly vitreous system Bi2O3–B2O3–BaO: Structural, morphologic, and thermal analysis. Optical Materials, 149, 115079.

[26] M. Boulares, B. Chamam, A. Mejri, M.A. Wahab, A. Haddouk, L. El Mir, A.H. Hamzaoui, A. Kallel, C. Tizaoui, I. Trabelsi, Robust magnetic γ-Fe2O3/Al–ZnO adsorbent for chlorpyriphos removal in water. Water 14, 1160 (2022). https://doi.org/ 10.3390/W14071160

[27] I Ben-Amor, H. Hemmami, S.E. Laouini, M.S. Mahboub, A. Barhoum, Sol-gel synthesis of ZnO nanoparticles using different chitosan sources: efects on antibacterial activity and photocatalytic degradation of AZO dye. Catalysts (2022). https://doi.org/ 10.3390/CATAL12121611

[28] Farooq, N., Khan, M. I., ur Rehman, Z., Wattoo, M. A., Qureshi, A. M., Shanableh, A., & ur Rehman, A. (2024). Barium-doped ceria-fabricated graphitic carbon nitride (BDC/g-

C3N4) nanomaterial as improved photocatalyst for efficient vitiation of organic dyes from industrial effluents. Inorganic Chemistry Communications, 159, 111830.

[29] Farooq, N., Hussain, S., Alkorbi, A. S., Qureshi, A. M., Wattoo, M. A., Alsaiari, R., ... & ur Rehman, A. (2022). Efficient electrochemical and photocatalytic performances of Cu-doped BaxAlxO3 nanocomposites. Surfaces and Interfaces, 32, 102116.s